CHEMISTRY
A EUROPEAN JOURNAL

DOI: 10.1002/chem.201000413

Kinetic Stability and Propellant Performance of Green Energetic Materials

Martin Rahm[a, b] and Tore Brinck*[a]

Abstract: A thorough theoretical investigation of four promising green energetic materials is presented. The kinetic stability of the dinitramide, trinitrogen dioxide, pentazole, and oxopentazole anions has been evaluated in the gas phase and in solution by using high-level ab initio and DFT calculations. Theoretical UV spectra, solid-state heats of formation, density, as well as propellant performance for the corresponding ammonium salts are reported. All calculated properties for dinitramide are in excellent agreement with experimental data. The stability of the trinitrogen dioxide anion is deemed sufficient to enable synthesis at low temperature, with a barrier for decomposition of approximately 27.5 kcal mol^{-1} in solution. Oxopentazolate is expected to be approximately 1200 times more stable than pentazolate in solution, with a barrier exceeding 30 kcal mol^{-1}, which should enable handling at room temperature. All compounds are predicted to provide high specific impulses when combined with aluminum fuel and a polymeric binder, and rival or surpass the performance of a corresponding ammonium perchlorate based propellant. The investigated substances are also excellent monopropellant candidates. Further study and attempted synthesis of these materials is merited.

Keywords: density functional calculations · energetic materials · green chemistry · kinetics · propellants

Introduction

Environmentally compatible green energetic materials are a topic of intense research worldwide.[1,2] Novel high-energy-density materials (HEDMs) synthesized in recent years, such as hexanitrohexaazaisowurtzitane (CL-20), various tetrazole- and tetrazine-based salts, nitrated cubanes, furazans, and furoxans have been suggested for ranges of applications such as primary and secondary explosives,[3,4] pyrotechnics,[5] propellant formulations, and so forth.[1,2,4]

As opposed to a typical explosive, an oxidizer is a molecule with a positive oxygen balance. Oxidizers suitable for solid rocket propellants are very few in numbers and the majority of formulations used today are based on ammonium perchlorate (AP, NH_4ClO_4). Environmental concerns have been pushing the development towards a new generation of green propellants. Ammonium dinitramide (ADN, $NH_4N(NO_2)_2$) is one of the more promising oxidizers for this purpose.[1]

The design, synthesis, and characterization of new high-nitrogen compounds are very difficult due to their energetic nature. The inherent instability of nitrogen-rich molecules arises from the very large thermodynamic driving force for N_2 gas production, as an N–N bond ($\approx$38 kcal mol^{-1}) or N=N bond ($\approx$100 kcal mol^{-1}) is transformed into an N$\equiv$N bond ($\approx$228 kcal mol^{-1}). What separates a potential useful molecule from one that is not is the rate at which this transformation occurs, the kinetic stability. Therefore, quantum chemical studies are key in predicting decomposition rates and precede synthetic efforts. Ideally an HEDM suitable for handling at room temperature should have a free-energy activation barrier for decomposition that exceeds roughly 30 kcal mol^{-1}. This value is estimated assuming first-order decomposition kinetics, and corresponds to a half-life of 35 years at room temperature. However, smaller barriers can be acceptable under low-temperature conditions.

Stable and metastable high-nitrogen and -oxygen compounds are naturally of large academic interest. However, knowledge of the stability and mere nitrogen/oxygen content is insufficient if one wants to assess a compound's potential practical use as an explosive or propellant; a potential species also needs to exhibit good performance characteristics. In the case of propellant formulations these include

[a] M. Rahm, Prof. T. Brinck
Physical Chemistry, School of Chemical Science and Engineering
Royal Institute of Technology (KTH), 10044 Stockholm (Sweden)
Fax: (+46) 08790-8207
E-mail: tore@physchem.kth.se

[b] M. Rahm
Competence Centre for Energetic Materials (KCEM)
Gammelbackavägen 6, 69151 Karlskoga (Sweden)

combustion parameters such as specific impulse and combustion temperature. Information regarding these can be theoretically obtained using different program codes, by typically utilizing free-energy minimization.

This work is focused on four energetic anions (Scheme 1) with varying oxygen content; the dinitramide anion $[N(NO_2)_2]^-$, the trinitrogen dioxide anion $[N(NO)_2]^-$, the pentazole anion (or pentazolate) $[N_5]^-$, and the oxopentazole anion (or oxopentazolate) $[ON_5]^-$. Depending on the choice of counterions, these species can be tuned to either explosive or propellant applications. In addition to investigating the kinetic stability of these anions in the gas phase and solution we have theoretically estimated their potential as solid rocket propellants in conjunction with the ammonium cation $[NH_4]^+$.

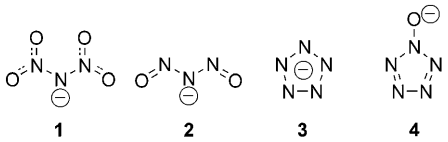

1 2 3 4

Scheme 1. The dinitramide (**1**), trinitrogen dioxide (**2**), pentazole (**3**), and oxopentazole (**4**) anions.

Dinitramide and trinitrogen dioxide: The stability of dinitramide salts is a highly complex issue, and the experimentally determined decomposition barrier of solid-state ADN is typically reported in the range of 29 to 42 kcal mol^{-1}.[6–10] However, the decomposition barrier for the free dinitramide anion (c.f. **1** in Scheme 1) has been theoretically estimated to be 47 kcal mol^{-1}.[9,10] The large barrier can be attributed to stabilization of the anion through considerable electron-resonance delocalization. The actual real-life stability of **1** is strongly coupled to its ability to polarize charge, and its chemical environment has been shown to be of great importance.[9,10] In addition, phase transitions due to eutectics of dinitramide salts with their corresponding nitrate decomposition products further complicate the thermal behavior.[8–10] The stability of dinitramide anions in common solvents is typically good. However, theoretical estimations of solvated decomposition kinetics have not been reported.

The trinitrogen dioxide anion (see **2** in Scheme 2 below), which is structurally related to **1**, was first detected by Moruzzi and Dakin in 1968 in drift cell experiments.[11] Its existence in the gas phase has since been corroborated by several groups.[12–14] The stability of **2**, relative to $NO+N_2O+e^-$, has been measured to be (2.0 ± 0.2) eV ((46 ± 4.6) kcal mol^{-1}) using coincident photoelectron and photofragment translational spectroscopy.[13] Collision-induced dissociation studies also support the existence of an isomer with an estimated stability of (0.76 ± 0.1) eV ((18 ± 2.3) kcal mol^{-1}).[14] There is also evidence to suggest an isomer with a bond strength of approximately 1.3 eV (30 kcal mol^{-1}),[14] as well as a weakly bound $[NO–N_2O]$ cluster bonded by approximately 0.2 eV (5 kcal mol^{-1}).[15] Despite its apparent stability in the gas phase, no attempts to chemically synthesize **2** have been reported, and no detection or characterization of the ion in solution is known.

It should be noted that several theoretical studies of trinitrogen dioxide isomers have been undertaken.[12,14,16–18] However, little correlation with the experimental results have been achieved. For instance, the high stability of the valence-bound isomer **2** has not been reproduced theoretically. Low-level calculations on the structure and stability of several different weakly bound $[NO–N_2O]^-$ complexes further confuse the situation.

A deeper understanding of the criteria for kinetic stability in nitrogen- and oxygen-rich structures such as these is important, not only because of the high relevance of dinitramides as oxidizers and in explosives, but also for the progress of energetic materials research in general. We have performed a thorough quantum chemical study of the dinitramide anion (**1**) and the trinitrogen dioxide anion (**2**) in the gas phase, as well in solutions in THF. Kinetic stability, performance characteristics of **1** and **2**, and possible routes to the synthesis of **2** are discussed.

Pentazoles: The successful synthesis of the chainlike N_5^+ cation in 1999 by Christe and co-workers[19] sparked renewed interest in all nitrogen compounds. Extensive theoretical and experimental work on the cyclic pentazole anion (N_5^-, c.f. **3** in Scheme 1) resulted in its detection in the gas phase by mass spectroscopy in 2002[20] and 2003.[21] The decomposition barrier for the cyclic N_5^- anion has been estimated to be 26 kcal mol^{-1} by using high-level ab initio calculations.[21] As the detection of the pentazole anion in the condensed phase by NMR spectroscopy has proven difficult[22–24] it is still a topic of ongoing research.[25–27]

The stability of many aryl pentazoles is well established; their decomposition barriers are typically around 20 kcal mol^{-1}.[25,28–30] Other pentazole compounds are also known. Hammerl and Klapötke have, for instance, shown the existence of tetrazolylpentazole by using low-temperature $^{15}N/^1H$ NMR spectroscopy.[31] The stability of tetrazolylpentazole and its corresponding anion pentazolyltetrazolate was calculated to be 15–16 and 21–22 kcal mol^{-1}, respectively, using B3PW91 and MP2 calculations,[31] and later to be 11.4 and 17.7 kcal mol^{-1}, respectively, using CCSD(T) calculations.[32]

An interesting and poorly understood molecule in the pentazole family, with possible applicability as an HEDM, is the cyclic oxopentazole anion (ON_5^-, c.f. **4** in Figure 5 below). Cheng et al. have previously considered this molecule very briefly, together with other XN_5^- (X=S, Se, and Te) derivatives.[33] The barrier for concerted cleavage of ON_5^- into N_2O and N_3^- in the gas phase was then estimated to be 32.7 kcal mol^{-1} at the B3LYP/6-31+G* level. The calculation of nuclear-independent chemical shifts (NICS) and the existence of $4n+2\pi$ electrons also confirmed the aromatic nature of the ring.[33] Hammerl et al. have investigated the isoelectronic neutral FN_5 molecule using CCSD(T) calculations, and predicted a decomposition barrier of 6.7 kcal mol^{-1}.[32] Very recently, Noyman et al. investigated

the effect of separating the σ and π molecular orbitals (MOs) of polynitrogen systems by introducing oxygen atoms.[34] Among other things they concluded that coordination of oxygen to the nitrogen ring system of pentazolate (**3**) did not stabilize the molecule (i.e., oxopentazolate, **4**). The lowest transition state leading away from **4** is reported to be only 25.2 kcal mol^{-1} higher than the ground state at the B3LYP/cc-pVDZ level, thereby producing two N_2 molecules and one NO^- anion.[34]

We found it prudent to make a more thorough investigation into the kinetic stability and performance of this exotic molecule, and to compare it with the pentazole anion (**3**).

Results and Discussion

Kinetic stability in the gas phase and in THF

Dinitramide: As already mentioned in the Introduction, the behavior of solid-state dinitramide salts is a complex issue due to charge polarization, surface chemistry, and phase transitions. Fortunately, the behavior in solution is likely to be more easily understood due to the removal of specific interactions with the counterions (NH_4^+ in the case of ADN) that are present in the crystal lattice and on crystal surfaces. Thus we can assume that solvated dinitramide salts are sufficiently described using only the free dinitramide anion in a single-solvent medium. Solute–solvent energies can then be estimated using implicit solvation models (such as the polarizable continuum model (PCM) or conductor-like screening model (COSMO)).

Two possible decomposition routes have been considered for the free dinitramide anion (Figure 1). Firstly, the direct transformation into nitrate and nitrous oxide through **TS1**, secondly a bond cleavage into the NNO_2 radical anion and nitrogen dioxide (**1**→**5**). In the gas phase the lowest-energy pathway appears to be **TS1**, requiring an enthalpy of activation of 46 kcal mol^{-1}. However, the dissociative pathway is likely to be in close competition, due to its more favorable change in entropy.

More important is the behavior in solution. As shown in Figure 1, solvation by THF stabilizes the smaller NNO_2 radical anion and nitrogen dioxide (**5**), relative to the dinitramide anion (**1**), and lowers the dissociative barrier by more than 7 kcal mol^{-1}, which results in an enthalpy of activation of 42 kcal mol^{-1}. The process is a pure dissociation, that is, the maximum energy along the reaction coordinate is reached at infinite separation of the two resulting species. This was shown using a high-resolution scan of the nitrogen–nitrogen SCF energy surface at the UB3LYP/6-31+G(d) level, using the default PCM model of Gaussian 03.[44] The entropic gain associated with dissociation due to additional degrees of freedom as one species is transformed into two is likely to decrease the actual barrier height by a few kilocalories. Thus, the decomposition barrier for dinitramide anions in low and medium polarity solvents will be in the vicinity of 40 kcal mol^{-1}, in good agreement with experimental estimates for several solid and molten dinitramide salts.[35]

Trinitrogen dioxide: Modeling the kinetic stability of the trinitrogen dioxide anion (c.f. **2** in Scheme 2) is a complex matter, mostly due to the proximity of different spin states. For this reason single-determinant wave function methods, such as HF and MP2, produce unreliable energies. This is unfortunate, because most of the theoretical work on the subject has been done using such methods.[12,14,16] We believe that the theoretical work presented here is an important step towards reaching a consensus on the trinitrogen dioxide paradigm.

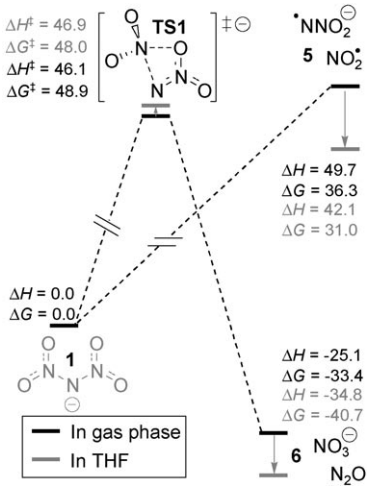

Figure 1. The decomposition of the free dinitramide anion (**1**) proceeds through intramolecular NO_2 transfer in the gas phase, and through nitrogen–nitrogen bond cleavage in THF solvent. Enthalpies of activation are 46.1 and 42.1 kcal mol^{-1}, respectively, when calculated at the CBS-QB3 level of theory.

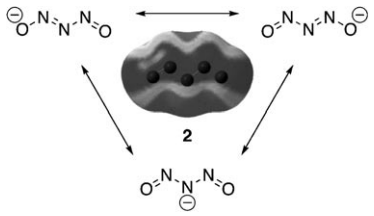

Scheme 2. The electrostatic surface potential of the trinitrogen dioxide anion (**2**) mapped onto a constant electron-density contour, after a B3LYP/6-31+G(d) calculation. Values ranging from −109.8 to −100.4 kcal mol^{-1}, together with selected electron-resonance structures indicate stabilization through considerable electron delocalization.

The trinitrogen dioxide anion (**2**) exhibits many similar structural and electronic traits to the dinitramide anion (**1**). Most important is electron-resonance delocalization, which is illustrated by Lewis structures and an electrostatic surface potential map in Scheme 2. The ability to evenly distribute charge ensures that the nitrogen–nitrogen bonds are strengthened relative to otherwise weaker single bonds. If

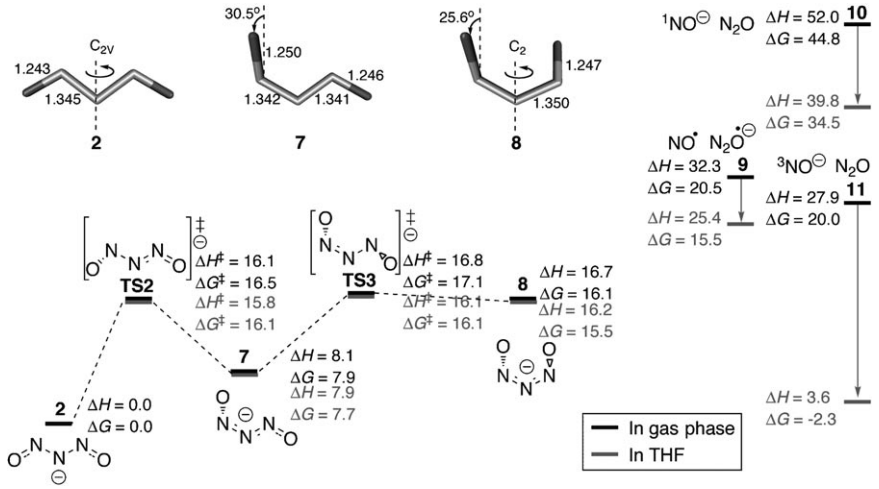

Figure 2. The rotational conformers **2**, **7**, and **8** of the trinitrogen dioxide anion, with interconnecting transition-state structures. The possible dissociation products **9**, **10**, and **11** are also shown. Bond lengths are shown in Ångström.

one considers the closed-shell singlet species, there are three rotational conformers of trinitrogen dioxide: **2**, **7**, and **8** (Figure 2). These are separated by rotational barriers with enthalpies of activation equaling 16 and 17 kcal mol^{-1}, respectively, which enables equilibration of the states at room temperature. The second conformer, **7**, lies 8 kcal mol^{-1} higher in energy than **2**, and is hence destabilized by an equal amount. The third conformer, **8**, has a much higher relative enthalpy of approximately 17 kcal mol^{-1}, and can be considered irrelevant from a thermodynamic point of view.

Looking at the potential energy surface (PES) leading away from **2**, there are four possible fractionation products to consider. These are shown in Equations (1)–(4) together with their zero-point-energy-corrected relative energies calculated at the CBS-QB3 level. Figure 2 also shows the corresponding relative enthalpies and free energies in the gas phase and in solution.

$$\mathbf{2} \longrightarrow \begin{cases} N_2O + {}^1NO^- & (+50.9\ \text{kcal mol}^{-1}) & (1) \\ N_2O + {}^3NO^- & (+26.7\ \text{kcal mol}^{-1}) & (2) \\ N_2O + NO^\bullet + e^- & (+27.0\ \text{kcal mol}^{-1}) & (3) \\ N_2O^- + NO^\bullet & (+50.9\ \text{kcal mol}^{-1}) & (4) \end{cases}$$

Resat et al. measured the energetics for Equation (3) and found it to be (46 ± 4.6) kcal mol^{-1} using photoelectron-photofragment coincidence spectroscopy measurements.[13] They concluded that this value may be taken as a measure of the stability of **2** if it is assumed that some of the $NO + N_2O$ products are produced with no internal excitation, and that the parent $N_3O_2^-$ molecule is cold. However, their measured value for Equation (3) is considerably higher than our computed value of 27.0 kcal mol^{-1} for the same process. The large discrepancy can hardly be attributed to an error in the computed value, since the computational approach is highly accurate (CBS-QB3), and therefore we find that the assumption of no internal excitation in the products must be questioned. Comparisons of experimental and computational data indicate that the $N_3O_2^-$ molecule observed in the experiment agrees well with the characteristics of cold **2**. On the basis of the photoelectron spectrum at 266 nm, the vertical and adiabatic ionization energies of $N_3O_2^-$ can roughly be estimated to be 3.1 and 3.8 eV, respectively; our computed values for **2** are 3.1 and 4.0 eV, respectively. Furthermore, radiation at 266 nm leads to photodissociation with NO, N_2, and O^- as the most probable products. According to computations, the only allowed electronic excitation in this region has an absorption maximum at 271 nm. Geometry optimization of the excited state indicates that the photon absorption indeed leads to dissociation into NO, N_2, and O^-.

Torchia et al.[14] have also questioned the assumption that vibrationally cold dissociation products are formed in the experiment reported by Resat et al. They argue that as much as 1.3 eV of vibrational energy is likely in the dissociation products at the threshold energy for photodetachment. The dissociation energy for Equation (2) was estimated to be 18 kcal mol^{-1} based on energy-resolved collision-induced dissociation experiments and ab initio calculations at the MP2 level. In light of the more accurate calculations presented here, it is advisable that the wealth of experimental data produced on this system is reexamined.

If one considers intramolecular chemical transformations on the singlet PES of trinitrogen dioxide, three transition states have been identified (Figure 3), all accessed through conformer **7**. The concerted formation of N_2 and an NO_2 anion, through **TS4**, is a highly exothermic reaction with a reaction enthalpy of −55.9 and −64.3 kcal mol^{-1} in the gas phase and THF, respectively. This process has an activation enthalpy of 32–33 kcal mol^{-1}, and will likely be one of the main decomposition pathways at elevated temperatures. **TS5** is calculated to be somewhat lower in energy than **TS4**, with an enthalpy of activation of 30 kcal mol^{-1}, and produces the loose $[NO–N_2O]^-$ cluster **13**. Diffuse functions (+) are needed in the basis set to converge onto this minimum. For this reason we have estimated its relative energy using the G2X extrapolation (instead of the composite CBS-QB3 method). It is important to note that **13** has a bonding enthalpy of 4.3 kcal mol^{-1}, relative to free NO and N_2O^- (**9**).

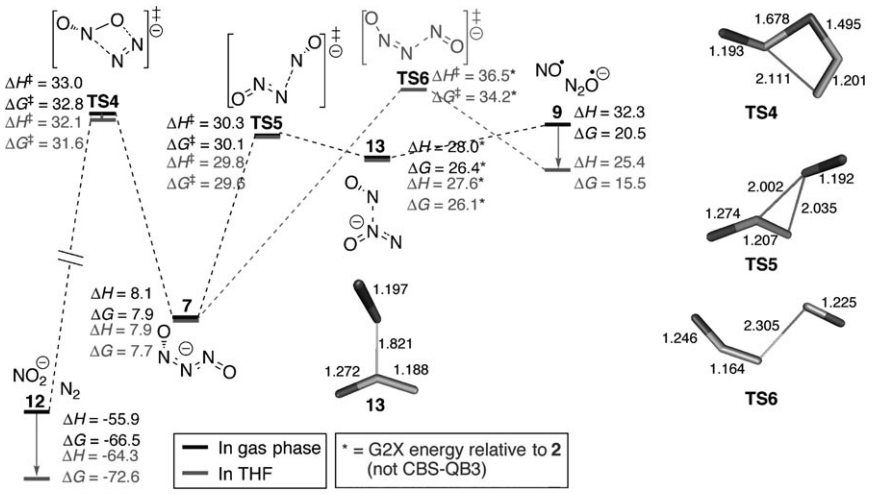

Figure 3. Three possible decomposition routes of conformer **7** are shown. All energies are given relative to **2** (Scheme 2). Bond lengths of selected species are shown in Ångström.

This value corresponds well with the experimental bond strength of 0.2 eV (4.6 kcal mol^{-1}), presented by Coe et al.[15]

As mentioned earlier, the true kinetics for decomposition of the trinitrogen dioxide anion is complicated by the proximity of different spin states. Equation (2) (**2**$\rightarrow{}^3NO^- + N_2O$) corresponds to the lowest bond-dissociation enthalpy (27.9 kcal mol^{-1}), compared to the other alternatives. However, it requires a change of spin, which is likely to slow down the process. Figure 4 shows the PES of **2** and **7** along the nitrogen–nitrogen dissociation reaction coordinate, both on the singlet and triplet surfaces, close to the crossing geometries. The B3LYP energies agree fairly well with the more accurate methods, and at longer distances the energies converge on the values for the dissociated products (i.e., **9** and **11**).

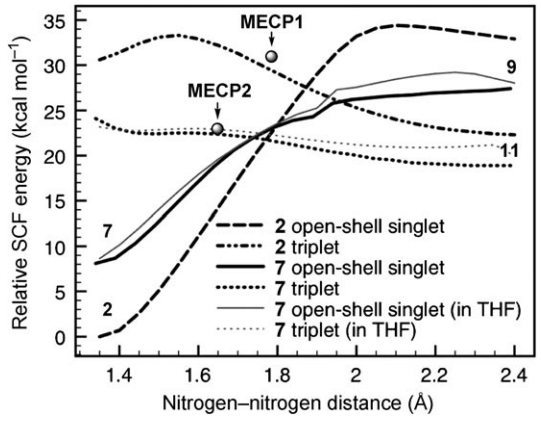

Figure 4. Scans of the nitrogen–nitrogen bond in **2** and **7** at the UB3LYP/6-31+G(d) level indicates the possibility of spin-forbidden intersystem crossing onto the triplet surface. Geometry-optimized minimum-energy crossing points (MECP) are indicated as dots. Scans of singlet and triplet **7** in THF are also shown. Lines converge towards **9** and **11**, for singlet and triplet states, respectively.

The minimum on the hyperdimensional seam of crossing between the singlet and triplet surfaces, the minimum-energy crossing point (MECP), is ideally localized using a multireference method such as CASSCF or MR-CI. However, we have instead performed broken-symmetry calculations with the less costly DFT B3LYP method. In many cases, single-reference methods, such as DFT, are known to work surprisingly well for this purpose.[36] In view of the lower level of theory used, we have not calculated the surface gradients and spin–orbit coupling matrix elements required for a full Laudau–Zener[36,37] treatment for the probability of crossing. It has, however, been estimated that spin-forbidden reactions are slower than spin-allowed by a factor of 1 to 4 orders of magnitude.[36] Close to room temperature this corresponds to raising an adiabatic reaction barrier by 1.4 to 5.5 kcal mol^{-1}. By using this estimate, and our calculated relative energies of **MECP1** and **MECP2** in Figure 4, we can make a crude comparison to other reaction barriers. We will leave it for future work to decipher the spin-forbidden process at a higher level of theory.

MECP2 is the lowest crossing point leading away from **2** (via **7**), and has a relative energy of 22.4 kcal mol^{-1} after a B3LYP/6-31+G(d) optimization. A single-point calculation at the CCSD(T)/6-311+G(2df) level raises this energy to 24.0 kcal mol^{-1}. However, at this level of theory and geometry, the triplet energy lies above the singlet by 6.0 kcal mol^{-1}, which indicates that the B3LYP crossing is too early, that is, the energy and the nitrogen–nitrogen distance of the real crossing should be higher. In the gas phase this is of less importance as the triplet surface at long distances approaches the higher value corresponding to **11** (Figure 2). That is, the rate-determining enthalpy barrier for **2** in the gas phase should exceed at least 27.9 kcal mol^{-1}. Adapted frequency analysis showed that both crossing points are minima on the 3N–7 dimensional seam of crossing. By using the obtained frequencies, the enthalpy correction for **MECP2**, relative to **2**, was calculated to be −2.7 kcal mol^{-1}.

MECP2 could be of greater importance for the kinetics in solution, as the triplet surface dramatically drops in energy at larger distances (Figure 2). Figure 4 shows that the crossing point should be very similar in geometry in going from the gas phase to solution, and single-point calculations at several levels of theory support this. The relative solvation energy for **MECP2** was calculated to be +4.8 kcal mol^{-1} at the B3LYP/6-31+G(d) level. A most conservative estimate of a corresponding adiabatic enthalpy barrier in solution is thus given by 24.0+1.4−2.7+4.8=27.5 kcal mol^{-1}.

We can conclude that, in contrary to several other computational studies on the matter of trinitrogen dioxide, our calculations offer a strong complement to the experimental work by Resat et al.,[13] Torchia et al.,[14] and Coe et al.[15] The barrier for decomposition in the gas phase is close to 30 kcal mol^{-1}. Larger as well as significantly smaller experimental bond strengths can be explained using different rotational conformers, loose complexes, and a strong photon absorption at 271 nm. A spin-forbidden intersystem crossing process likely governs the kinetics in solution. Our most conservative estimate puts the stability of **2** in solution in the same range as that of the pentazole anion. However, as the stability could be higher, more advanced multireference calculations should be attempted. Regardless, the trinitrogen dioxide anion (**2**) appears to have a sufficient kinetic stability to enable synthesis and experimental detection at reasonable temperatures.

Pentazolate: The stability of the pentazole anion (**3**) has been thoroughly investigated theoretically by several groups[20–22,27,30,38] and requires little additional comment. Our calculations on **3** were primarily performed to enable comparison with oxopentazolate (see **4** in Figure 5).

Scheme 3 shows the concerted ring opening of **3**, through **TS7**, which requires an enthalpy of activation of 28 kcal mol^{-1}. In THF the solvent appears to stabilize the ground state relative to the transition state, with approximately one kilocal per mole. The product species, nitrogen gas and azide (**14**), lie 9 and 14 kcal mol^{-1} below **3** in the gas phase and THF, respectively.

Oxopentazolate: The oxopentazole anion (**4**) is found to be considerably more stable than the parent pentazolate (**3**). Figure 6 shows three decomposition routes for **4**. The previously considered concerted rupture into nitrous oxide and azide (**15**) through **TS8** has an enthalpy of activation of 38 kcal mol^{-1} in the gas phase. This is a significantly higher barrier than the 33 kcal mol^{-1} reported by Cheng and Li.[33] However, knowledge of this transition state alone is insufficient if one wants to describe the kinetic stability of the molecule. Since **4** is of a lower symmetry than **3**, additional decomposition pathways exist.

Rigorous work was done in identifying all transition structures leading away from the ground state, including scans of the PES along all nitrogen–nitrogen bonds. The lowest, and hence most relevant, transition

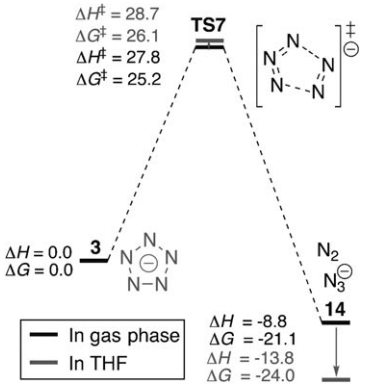

Figure 5. The stability of pentazolate (**3**) is increased slightly in THF, relative to the gas phase. The enthalpy of activation changes from 27.8 to 28.7 kcal mol^{-1}, at the CBS-QB3 level of theory.

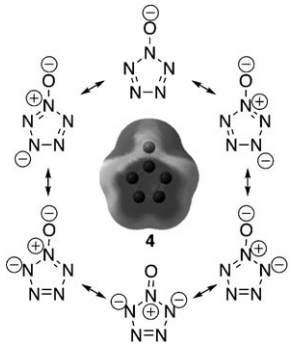

Scheme 3. The electrostatic surface potential of oxopentazolate (**4**) mapped onto a constant electron-density contour, after a B3LYP/6-31+G(d) calculation. Values ranging from −109.8 to −100.4 kcal mol^{-1}, together with selected electron-resonance structures indicate stabilization through considerable electron delocalization.

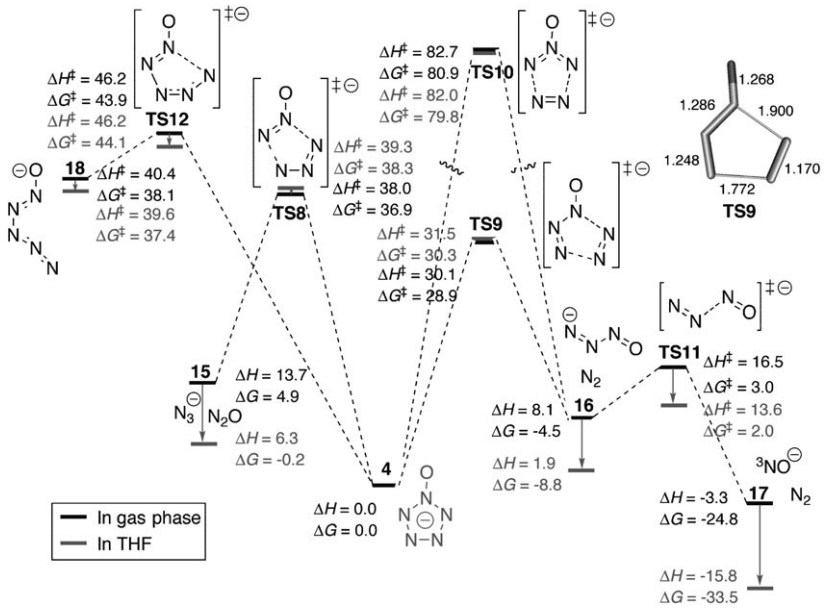

Figure 6. The kinetic stability of **4** has been investigated using high-level ab initio CBS-QB3 calculations. The lowest transition-state structure (**TS9**) for decomposition has a relative Gibbs free energy of 28.9 kcal mol^{-1} relative to **4** in the gas phase and exceeds 30 kcal mol^{-1} in low-polarity solvents.

state leading away from **4** is **TS9**. This transition state corresponds to an enthalpy of activation of 30.1 kcal mol^{-1} in the gas phase and 31.5 kcal mol^{-1} in THF, and produces nitrogen gas and the unstable trinitrogen oxide anion (**16**), which is likely to rupture into one additional nitrogen molecule and a nitrogen oxide anion (**17**) through **TS11**.

It was noted that the recently published calculations on a **4**→$2N_2+NO^-$ transition state[34] does not include a frequency analysis of the obtained geometry. Unfortunately the reported geometry is not optimized, which results in an activation barrier that is too low. Upon optimization, the applied C_s symmetry constraints prevent the correct transition state (**TS9**) from being found. Frequency analysis performed by us on the reported transition-state geometry, as well as the one obtained after optimization results in two imaginary frequencies. The optimized C_s geometry lies 6 kcal mol^{-1} above **TS9**. This is fortunate for the stability of **4**, as it would appear that the direct concerted formation of two nitrogen molecules is impossible, and the actual decomposition occurs through the following: N_5O^- (**4**)→**TS9**→$ON_3^-+N_2$ (**16**)→**TS11**→N_2+NO^- (**17**) (Figure 6).

When comparing the rate-determining **TS9** barrier height with **TS7** of **3** (pentazolate), **4** appears 500 times more stable in the gas phase and 1200 times more stable in THF. The interest in the pentazole anion (**3**) is motivated by the existence of arylpentazoles. Considering the extensive experimental efforts put into the detection of this species, our results show that synthesis of oxopentazolate is a reasonable quest worth pursuing.

Absorption spectra: Theoretical UV absorption spectra were obtained for anions **1**, **2**, and **4** in the gas phase. The highest probability transitions (in nm) are shown in Table 1. The pentazole anion (**3**), however, has no allowed transitions in this region.

Due to the very small changes in geometry for all ground-state species in going from the gas phase to solution, electronic structures, and hence calculated electronic transitions, are likely to be similar in both environments. In the case of the dinitramide anion (**1**), which, as opposed to the other anions, has several transitions of higher probability, our gas-phase calculations are within 5 nm of the experimental aqueous UV/Vis spectra of ADN.[39] The solvation effect on the excitation energies were further tested for all anions using time-dependent TD-B3LYP calculations together with a standard PCM procedure. The largest difference was seen for **3**, where the transition wavelength increased by 7 nm when going from the gas phase to a solution in THF. The corresponding corrections for **1** and **4** were smaller than 1 nm. Thus, the presented values at the CC2 level in the gas phase (Table 1) are expected be close to the real values in solution.

The presented calculated UV absorption bands allow for easy detection of both the trinitrogen dioxide anion (**2**) and oxopentazolate (**4**) upon formation. This is a great analytical advantage that is not available in the experimental efforts aimed at producing the long sought pentazole anion (**3**).

Propellant performance: For practical reasons a solid rocket propellant typically consists of a 70:30 weight mixture of ammonium perchlorate (AP) oxidizer and aluminum (Al) fuel. In addition to the oxidizer and the fuel a polymer matrix is also needed. In AP-based propellants cross-linked hydroxyl-terminated polybutadiene (HTPB) is typically used for this purpose. However, the most suitable type of matrix varies depending on the used oxidizer, and oxygen deficient but highly energetic anions such as **2**, **3**, and **4** should preferably be used with more oxygen-rich matrices to reach their peak performance. For this reason we have chosen to include 10 wt% glycidyl azide polymer (GAP)[40] in all our specific impulse calculations (Figure 7). This value is meant to correspond to a minimum required amount in a working formulation, and should preferably be optimized to reach an exact performance estimate. By comparison with the AP/Al reference we can estimate the difference in per-

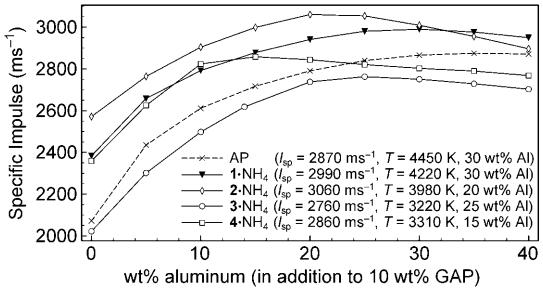

Figure 7. Calculated specific impulses (I_{sp}) of HEDMs **1** to **4** with ammonium counterions and AP are shown at different loadings of aluminum fuel and 10 wt% GAP binder. Maximum theoretical performances and corresponding combustion chamber temperatures and aluminum loadings are given within parentheses.

Table 1. Calculated properties of energetic anions **1** through **4**, and their corresponding ammonium salts.

Compound	Oxygen balance[a]	Relative stability in THF[b]	Density[a,c] [g cm^{-3}]	$\Delta H^0_{f,anion(vac)}$ [kcal mol^{-1}]	$\Delta H^{0\,[a,c]}_{f(s)}$ [kcal mol^{-1}]	A_{max}[d] [nm]	E_I[e] [eV]
1	+25.8	5.8×10^{11}	1.8 (1.8[36])	−31.2	−36.2 (−35.4[37])	279 (0.11)	4.4
2	±0.0	≈1[f]	1.6	13.0	2.9	271 (0.40)	3.1
3	−36.4	1	1.5	58.2	47.9	–	4.7
4	−15.3	1200	1.6	53.1	45.6	240 (0.20)	3.8

[a] Calculated for the corresponding ammonium salt. [b] Estimated from calculated room-temperature rate constants, obtained from free-energy barriers in solution. [c] Experimental data is given within parenthesis. [d] Calculated at the CC2/aug-cc-pVTZ level. Oscillator strengths are given within parentheses. [e] Adiabatic ionization energies are calculated at the B2PLYP/aug-cc-pVTZ level, with thermodynamic corrections from B3LYP/6-31+G(d) frequency analysis. [f] Rough estimate, possibly considerably more stable.

formance when using the energetic anions **1**–**4** instead of perchlorate.

Figure 7 shows calculated specific impulse (I_{sp}) values for the ammonium salts of **1**–**4** and AP after a nozzle expansion from 7 to 0.1 MPa (1 atm), at varying loadings of Al fuel. **1**·NH_4, or ADN, outperforms the reference by more than 4% at the same level of Al loading (30 wt%). This is slightly lower than the 8% proposed by other authors.[2] The deviation is likely due to differences in the considered formulations as well as the method of calculation. The chamber combustion temperature (T_c) is slightly lower than the reference, that is, 4220 K.

2·NH_4 reaches its maximum potential at 20 wt% loading of Al, at which it outperforms the reference by 7% and achieves an I_{sp} of 3060 m s^{-1} with a corresponding T_c of 3980 K. At 0% Al loading, ammonium trinitrogen dioxide is expected to outperform the other compounds due to its perfect oxygen balance, and achieve an I_{sp} of 2570 m s^{-1} at a T_c of only 2910 K. The high performance at low fuel loading and the low combustion temperature makes this compound relevant as a monopropellant.

3·NH_4 is less suitable for propellant applications, as it provides a performance slightly lower than the AP/Al reference. This is expected, as the pentazole anion does not contain any oxygen that can react with the metal fuel. After a successful synthesis of the pentazole anion, it is likely to find its main usage in explosive applications.

4·NH_4 clearly shows the effect of added oxidative power (oxygen) of the energetic anion on performance, relative to the oxygen-free pentazolate (**3**). Ammonium oxopentazole reaches its maximum potential at 15 wt% loading of Al, where it provides a performance almost identical to the reference, at a significantly lower T_c (3710 K). If used as a monopropellant the compound is expected to achieve an I_{sp} of 2360 m s^{-1} at the exceptionally low temperature of 2420 K.

Synthesis: It is not within the scope of this work to provide a feasible synthesis path to either of the discussed ions. However, we intend to briefly discuss some of our observations and ideas on the matter.

Since **2** has already been experimentally observed in the gas phase, and our theoretical investigations point to a reasonable stability as well as an excellent performance, it is a highly interesting anion to pursue for future HEDMs. Similar to the case in the gas phase, one can envision **2** being formed in solution through the exotic reaction between reduced nitrous oxide and nitrogen monoxide [Eq. (5)]. This reaction would be exothermic by 25 kcal mol^{-1} in THF (Figure 2) and provide a rapid route to **2**. The crux of the matter is naturally the reduction of nitrous oxide and the inherent instability of N_2O^- towards O^- and N_2 formation, which is known to proceed very rapidly.[41]

$$N_2O^- + NO \rightarrow [N_3O_2]^- \quad \Delta H^0_{THF} = -25.4 \text{ kcal mol}^{-1} \qquad (5)$$

In a more likely approach, **2** can be expected to form if hyponitrite anions (NO^-) are generated in the presence of nitrous oxide [Eq. (6)]. Templating by using metal catalysts or hydrogen-bonding counterions might also present other, more viable pathways to the formation of **2**.

$$N_2O + NO^- \rightarrow [N_3O_2]^- \quad \Delta H^0_{THF} = -3.6 \text{ kcal mol}^{-1} \qquad (6)$$

The synthesis of the pentazole anion has been suggested and attempted using substituted aryl pentazoles as precursors.[21,23,29] Future computational studies should be able to show if selective oxidation of aryl pentazoles is possible. If so, they could constitute a viable pathway to oxopentazolate.

Furthermore, the pentazole anion (**3**) is expected to form strong ferrocene-like sandwich complexes in the presence of metal cations (e.g., Fe^{2+}),[38] which should favor its formation in solution. Since it is not inconceivable that the same might apply for oxopentazolate (**4**), experimentalists attempting synthesis should consider including metal ions also in this case.

Conclusion

We have estimated the kinetic stability in the gas phase and in solution of four energetic anions—the commercially available dinitramide anion, the intensively pursued pentazole anion, its close relative the oxopentazole anion, and the trinitrogen dioxide anion—by using high-level ab initio and DFT calculations. The activation barrier to decomposition of oxopentazolate is estimated to be 30 kcal mol^{-1} in the gas phase and in solution, which corresponds to sufficient kinetic stability to enable synthesis, analysis, and handling at room temperature. The trinitrogen dioxide anion has a barrier for decomposition larger than 27.5 kcal mol^{-1} in solution. Detection of trinitrogen dioxide and oxopentazolate appears straightforward as they are predicted to exhibit strong UV absorption bands at 271 and 240 nm, respectively.

Calculated heats of formation for the gas-phase ions as well as their solid-state ammonium salts are reported. Theoretical rocket propellant performances with aluminum fuel show that ammonium trinitrogen dioxide and ammonium oxopentazole would outperform a standard ammonium perchlorate propellant at significantly lower combustion temperatures. The compounds are also predicted to perform well as monopropellants. Further study and attempted synthesis of these materials are merited.

The synthesis of oxopentazolate and trinitrogen dioxide presents formidable challenges to experimentalists. However, considering the strong environmental incentive to replace toxic energetic materials, and the successes of recent years in high-nitrogen synthesis, we can afford some optimism.

Computational Methods

The highly accurate multicomponent complete basis set (CBS-QB3)[42,43] method of Montgomery, Ochterski, and Peterson was used for obtaining energetics in the gas phase, using the Gaussian 03[44] program. CBS-QB3 uses coupled cluster (CCSD(T)) energies, which are extrapolated to the basis-set limit using MP2 and MP4 energies and empirical corrections. Geometries and thermodynamic corrections were obtained at the B3LYP/6-311G(d,p) level.[42,43] CBS-QB3 has been extensively tested in several benchmarks and is expected to produce reliable results.[42,43,45–47] The mean absolute deviation in the G2 test set is reported to be 0.87 kcal mol^{-1}.[42] The accuracy in predicting kinetics of pericyclic reactions is most important to our study. Guner et al. evaluated this for 11 different reactions[46,47] and CBS-QB3 was found to have a mean absolute deviation value of 1.9 and a standard deviation of 1.6 kcal mol^{-1}, when compared to experimentally determined activation enthalpies.

The B2PLYP[48] double-hybrid exchange-correlation functional by Swabe and Grimme, included in the ORCA[49] program suite, was also applied using an aug-cc-pVTZ basis. B2PLYP provide highly accurate energetics, for example, the mean absolute deviation for the G3/05 test set is 2.5 kcal mol^{-1} with a polarized QZV basis.[50] Relative energies in the gas phase were calculated for 298 K and 1 atm.

In some cases, in which diffuse functions were required during optimization, we employed a G2-type extrapolation scheme,[51,52] which we will refer to as G2X [Eq. (7)]. G2X has been used with B3LYP/6-31+G(d) geometries and frequencies. The accuracy for this type of method is expected to be within 2 to 3 kcal mol^{-1}.[51,52]

$$\Delta E(\mathrm{G2X}) = \Delta E(\mathrm{MP2/6\text{-}311{+}G(3df,2p))} - \Delta E(\mathrm{MP2/6\text{-}31+G(d')}) + \Delta E(\mathrm{CCSD(T)/6\text{-}31{+}G(d')}) \quad (7)$$

Absorption spectra for the free anions in the gas phase were obtained through CC2[53]/aug-cc-pVTZ calculations on the four lowest-lying excitations, using the turbomole code.[54] Gas-phase calculations on the dinitramide anion produce excitations in excellent agreement with experimental aqueous measurements.[39] The effects of THF solvent were analyzed at the td-RB3LYP/6-31+G(d) level of theory using the default PCM method of Gaussian 03, and found to be minor. The rigidity of the CC2 method was also evaluated by comparison with experimental data available for the nitrate anion.[55] Excellent agreement was observed.

Solvation energies: To calculate reliable energies in THF solvent a quite extensive procedure was devised (Figure 8). To correct the gas-phase energies (at the CBS-QB3 level) for solvent effects, all geometries and thermodynamic corrections were recalculated in the gas phase and in THF at the B3LYP/6-31+G(d) level, using the default PCM method of Gaussian 03.[44] To obtain solvation energies (ΔG_{solv}) the obtained geometries were used in single-point calculations at the B2PLYP/aug-cc-pVTZ level, utilizing the COSMO solvation model in the ORCA program. These energies were then corrected for thermal and entropic effects using the frequencies calculated at the B3LYP level. Relative free energies in THF (ΔG^0_{THF}) were calculated for 1 M concentrations, and are given by Equation (8):

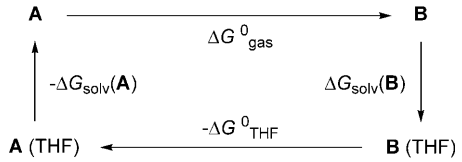

Figure 8. Thermodynamic cycle used for calculating relative free energies in solution (ΔG^0_{THF}). **A** denotes the reactant molecule and **B** a product or a transition state.

$$\Delta G^0_{THF} = \Delta G^0_{gas}(\mathrm{CBS\text{-}QB3}) + \Delta G_{solv}(\mathbf{B}) - \Delta G_{solv}(\mathbf{A}) \quad (8)$$

in which ΔG_{solv} for **A** and **B** were calculated as shown in Equation (9):

$$\Delta G_{solv} = E(\mathrm{B2PLYP/aug\text{-}cc\text{-}pVTZ(COSMO)//B3LYP/6\text{-}31{+}G(d),\ THF\ geometry}) + G_{corr}(\mathrm{B3LYP,\ THF\ geometry}) - E(\mathrm{B2PLYP/aug\text{-}cc\text{-}pVTZ//B3LYP/6\text{-}31{+}G(d),\ gas\text{-}phase\ geometry}) - G_{corr}(\mathrm{B3LYP,\ gas\text{-}phase\ geometry}) \quad (9)$$

Ionization potentials: Adiabatic ionization energies (E_I) in the gas phase were obtained from B3LYP/6-31+G(d)-optimized structures of anions **1**–**4** and their corresponding radicals, at the B2PLYP/aug-cc-pVTZ level of theory. The energies were corrected for thermal and entropic effects using B3LYP frequencies.

Density estimations: By considering only small cations (NH_4^+) and larger anions (**1**–**4**), and assuming efficient packing of the species in a solid lattice, an estimate of the salt density can be written as shown in Equation (10):

$$\rho_{salt} = (M_{anion} + M_{cation})/V \quad (10)$$

in which M_{anion} and M_{cation} are the molecular weights of **1**–**4** and NH_4^+, respectively, and V is the lattice volume, which is equal to the sum of the individual anion and cation volumes. The volumes for anions **1**–**4** were calculated from the 0.001 a.u. contour of their B3LYP/6-31G(d) electron density using Gaussian 03[44] and the HS95v09[56] program. For the NH_4^+ cation we instead used the experimentally determined volume[57] of 0.021 nm^3. A similar procedure has been successfully demonstrated for nitramine compounds,[58] and our results are in excellent agreement with experimental data, which is available for the ADN salt.[39]

Enthalpies of formation: Enthalpies of formation for the gas-phase ions ($\Delta H^0_{f(vac)}$) **1**–**4** were obtained at the CBS-QB3 level of theory. However, despite the high accuracy of the CBS extrapolation for relative energies, it proved somewhat lacking in its description of the exact energy for the nitrogen molecule. For this reason we instead chose to use azide (N_3^-) as our nitrogen reference. Dixon et al. have previously calculated $\Delta H^0_{f(vac)}$ for azide to be 47.4 kcal mol^{-1} at 298.15 K, using a more advanced CBS extrapolation scheme.[59] This value is in good agreement with gas-phase acidity measurements that gives a $\Delta H^0_{f(vac)}$ value of (48 ± 2) kcal mol^{-1}.[60] Heats of formation for solid salts ($\Delta H^0_{f(s)}$) were obtained through Equation (11):

$$\Delta H^0_{f(s)} = \Delta H(NH_4{}^+)^0_{f(gas)} + \Delta H(\mathrm{anion})^0_{f(gas)} + \Delta H_L \quad (11)$$

in which ΔH_L is the lattice enthalpy, which in the case of nonlinear polyatomic ions is given by Equation (12):[61]

$$\Delta H_L = 2U_L/RT \quad (12)$$

in which U_L is the lattice energies of the ionic solids. We have calculated U_L for the ammonium salts of anions **1**–**4** using a relationship [Eq. (13)] developed by Mallouk et al.,[61] which was later expanded by Jenkins et al.[62] and Gutowski et al.[57]

$$U_L = 2I[\alpha(V^{-1/3}) + \beta] \quad (13)$$

in which I is the ionic strength (equaling 1, for 1:1 salts), α and β are empirical constants (19.9 and 37.6 kcal mol^{-1} in the Gutowski method), and V is the sum of the ionic volumes (in nm^3), obtained as described in the previous section on density.

Equation (13) has been shown to be applicable to a wide range of 1:1 salts, and the Gutowski approach has recently been deemed the theoretical method of choice for estimating solid-phase heats of formation for energetic salts.[63]

Rocket propellant performance: The specific impulse, or effective exhaust velocity (I_{sp}), of a propellant is a most useful characteristic as it describes performance per mass of propellant. Specific impulses of the ammonium salts of anions **1** through **4** were estimated at varying loadings of aluminum (Al) fuel using NASA's CEA code,[64,65] assuming a chamber pressure of 7 MPa ($\approx$1000 psi) and a nozzle expansion to atmospheric pressure (0.1 MPa). The CEA code is based on known equations of states for thousands of known compounds, and assumes an equilibrium composition during expansion from an infinite area combustor. The calculation of specific impulses for unknown compounds can be performed after adding our calculated heats of formation to the CEA program's database. For polyglycidyl azide (GAP) a ΔH_f^0 value of 27.24 kcal mol^{-1} was used.[40]

Estimated chamber combustion temperatures (T_c) are also reported. These vary depending on the type of combustion that is predominant. For example, the formation of AlO_2 is a highly exothermic process, whereas more incomplete combustion will result in lower temperatures. T_c puts a practical limit on the type of material required in a rocket combustion chamber and nozzle, and lower temperatures allow for lighter and more affordable constructions.

Acknowledgements

The authors gratefully acknowledge the financial support given by the Swedish Research Council (VR), the Swedish Defence Research Agency (FOI), and Eurenco Bofors.

[1] J. Giles, *Nature* **2004**, *427*, 580–581.
[2] M. B. Talawar, R. Sivabalan, T. Mukundan, H. Muthurajan, A. K. Sikder, B. R. Gandhe, A. S. Rao, *J. Hazard. Mater.* **2009**, *161*, 589–607.
[3] R. P. Singh, R. D. Verma, D. T. Meshri, J. M. Shreeve, *Angew. Chem.* **2006**, *118*, 3664–3682; *Angew. Chem. Int. Ed.* **2006**, *45*, 3584–3601.
[4] K. O. Christe, *Propellants Explos. Pyrotech.* **2007**, *32*, 194–204.
[5] G. Steinhauser, T. M. Klapotke, *Angew. Chem.* **2008**, *120*, 3376–3394; *Angew. Chem. Int. Ed.* **2008**, *47*, 3330–3347.
[6] A. S. Tompa, *Thermochim. Acta* **2000**, *357–358*, 177–193.
[7] S. Vyazovkin, C. A. Wight, *J. Phys. Chem. A* **1997**, *101*, 5653–5658.
[8] A. N. Pavlov, V. N. Grebennikov, L. D. Nazina, G. M. Nazin, G. B. Manelis, *Russ. Chem. Bull.* **1999**, *48*, 50–54.
[9] M. Rahm, T. Brinck, *Chem. Commun.* **2009**, 2896–2898.
[10] M. Rahm, T. Brinck, *J. Phys. Chem. A* **2010**, *114*, 2845–2854.
[11] J. L. Moruzzi, J. T. Dakin, *J. Chem. Phys.* **1968**, *49*, 5000–5006.
[12] K. Hiraoka, S. Fujimaki, K. Aruga, S. Yamabe, *J. Phys. Chem.* **1994**, *98*, 8295–8301.
[13] M. S. Resat, V. Zengin, M. C. Garner, R. E. Continetti, *J. Phys. Chem. A* **1998**, *102*, 1719–1724.
[14] J. W. Torchia, K. O. Sullivan, L. S. Sunderlin, *J. Phys. Chem. A* **1999**, *103*, 11109–11114.
[15] J. V. Coe, J. T. Snodgrass, C. B. Freidhoff, K. M. McHugh, K. H. Bowen, *J. Chem. Phys.* **1987**, *87*, 4302–4309.
[16] A. Alijah, E. S. Kryachko, *J. Mol. Struct.* **2007**, *844–845*, 193–199.
[17] I. Papai, A. Stirling, *Chem. Phys. Lett.* **1996**, *253*, 196–200.
[18] A. Snis, I. Panas, *Chem. Phys. Lett.* **1999**, *305*, 285–292.
[19] K. O. Christe, W. W. Wilson, J. A. Sheehy, J. A. Boatz, *Angew. Chem.* **1999**, *111*, 2112–2118; *Angew. Chem. Int. Ed.* **1999**, *38*, 2004–2009.
[20] A. Vij, J. G. Pavlovich, W. W. Wilson, V. Vij, K. O. Christe, *Angew. Chem.* **2002**, *114*, 3177–3180; *Angew. Chem. Int. Ed.* **2002**, *41*, 3051–3054.
[21] H. Östmark, S. Wallin, T. Brinck, P. Carlqvist, R. Claridge, E. Hedlund, L. Yudina, *Chem. Phys. Lett.* **2003**, *379*, 539–546.
[22] R. N. Butler, J. C. Stephens, L. A. Burke, *Chem. Commun.* **2003**, 1016–1017.
[23] T. Schroer, R. Haiges, S. Schneider, K. O. Christe, *Chem. Commun.* **2005**, 1607–1609.
[24] R. N. Butler, J. M. Hanniffy, J. C. Stephens, L. A. Burke, *J. Org. Chem.* **2008**, *73*, 1354–1364.
[25] L. A. Burke, P. J. Fazen, *Int. J. Quantum Chem.* **2009**, *109*, 3613–3618.
[26] L. Belau, Y. Haas, S. Zilberg, *J. Phys. Chem. A* **2004**, *108*, 11715–11720.
[27] S. A. Perera, A. Gregusova, R. J. Bartlett, *J. Phys. Chem. A* **2009**, *113*, 3197–3201.
[28] R. N. Butler, A. Fox, S. Collier, L. A. Burke, *J. Chem. Soc. Perkin Trans. 2* **1998**, 2243–2248.
[29] P. Carlqvist, H. Oestmark, T. Brinck, *J. Phys. Chem. A* **2004**, *108*, 7463–7467.
[30] V. Benin, P. Kaszynski, J. G. Radziszewski, *J. Org. Chem.* **2002**, *67*, 1354–1358.
[31] A. Hammerl, T. M. Klapoetke, *Inorg. Chem.* **2002**, *41*, 906–912.
[32] A. Hammerl, T. M. Klapoetke, P. Schwerdtfeger, *Chem. Eur. J.* **2003**, *9*, 5511–5519.
[33] L. P. Cheng, X. Q. Li, *J. Mol. Model.* **2006**, *12*, 805–811.
[34] M. Noyman, S. Zilberg, Y. Haas, *J. Phys. Chem. A* **2009**, *113*, 7376–7382.
[35] S. B. Babkin, A. N. Pavlov, G. M. Nazin, *Russ. Chem. Bull.* **1997**, *46*, 1844–1847.
[36] J. N. Harvey, *Phys. Chem. Chem. Phys.* **2007**, *9*, 331–343.
[37] C. Wittig, *J. Phys. Chem. B* **2005**, *109*, 8428–8430.
[38] M. Lein, J. Frunzke, A. Timoshkin, G. Frenking, *Chem. Eur. J.* **2001**, *7*, 4155–4163.
[39] S. Venkatachalam, G. Santhosh, K. N. Ninan, *Propellants Explos. Pyrotech.* **2004**, *29*, 178–187.
[40] E. Diaz, P. Brousseau, G. Ampleman, R. E. Prud'homme, *Propellants Explos. Pyrotech.* **2003**, *28*, 101–106.
[41] H. U. Suter, T. Greber, *J. Phys. Chem. B* **2004**, *108*, 14511–14517.
[42] J. A. Montgomery, Jr., M. J. Frisch, J. W. Ochterski, G. A. Petersson, *J. Chem. Phys.* **1999**, *110*, 2822–2827.
[43] J. A. Montgomery, Jr., M. J. Frisch, J. W. Ochterski, G. A. Petersson, *J. Chem. Phys.* **2000**, *112*, 6532–6542.
[44] Gaussian 03, Revision C.02, M. J. Frisch, G. W. Trucks, H. B. Schlegel, G. E. Scuseria, M. A. Robb, J. R. Cheeseman, A. Montgomery, Jr., T. Vreven, K. N. Kudin, J. C. Burant, J. M. Millam, S. S. Iyengar, J. Tomasi, V. Barone, B. Mennucci, M. Cossi, G. Scalmani, N. Rega, G. A. Petersson, H. Nakatsuji, M. Hada, M. Ehara, K. Toyota, R. Fukuda, J. Hasegawa, M. Ishida, T. Nakajima, Y. Honda, a., O. Kitao, a., H. Nakai, a., M. Klene, a., X. Li, J. E. Knox, H. P. Hratchian, J. B. Cross, V. Bakken, C. Adamo, a., J. Jaramillo, R. Gomperts, R. E. Stratmann, O. Yazyev, A. J. Austin, R. Cammi, a., C. Pomelli, J. W. Ochterski, P. Y. Ayala, K. Morokuma, G. A. Voth, P. Salvador, J. J. Dannenberg, V. G. Zakrzewski, S. Dapprich, A. D. Daniels, M. C. Strain, O. Farkas, D. K. Malick, A. D. Rabuck, K. Raghavachari, J. B. Foresman, J. V. Ortiz, Q. Cui, A. G. Baboul, S. Clifford, J. Cioslowski, B. B. Stefanov, G. Liu, A. Liashenko, P. Piskorz, I. Komaromi, R. L. Martin, D. J. Fox, T. Keith, a., M. A. Al-Laham, C. Y. Peng, A. Nanayakkara, M. C., P. M. W. Gill, B. Johnson, W. Chen, M. W. Wong, C. Gonzalez, J. A. Pople, Gaussian, Inc. Wallingford CT, **2004**.
[45] D. H. Ess, K. N. Houk, *J. Phys. Chem. A* **2005**, *109*, 9542–9553.
[46] V. Guner, K. S. Khuong, A. G. Leach, P. S. Lee, M. D. Bartberger, K. N. Houk, *J. Phys. Chem. A* **2003**, *107*, 11445–11459.
[47] V. A. Guner, K. S. Khuong, K. N. Houk, A. Chuma, P. Pulay, *J. Phys. Chem. A* **2004**, *108*, 2959–2965.
[48] S. Grimme, *J. Chem. Phys.* **2006**, *124*, 034108.
[49] F. Neese, T. Schwabe, S. Grimme, *J. Chem. Phys.* **2007**, *126*, 124115/1–124115/15.
[50] T. Schwabe, S. Grimme, *Phys. Chem. Chem. Phys.* **2006**, *8*, 4398–4401.
[51] R. D. J. Froese, S. Humbel, M. Svensson, K. Morokuma, *J. Phys. Chem. A* **1997**, *101*, 227–233.
[52] L. A. Curtiss, P. C. Redfern, B. J. Smith, L. Radom, *J. Chem. Phys.* **1996**, *104*, 5148–5152.
[53] C. Hattig, *J. Chem. Phys.* **2003**, *118*, 7751–7761.

[54] TURBOMOLE V6.1 2009, a development of University of Karlsruhe and Forschungszentrum Karlsruhe GmbH, 1989–2007,TURBOMOLE GmbH, since 2007; available from http://www.turbomole.com.
[55] M. J. Blandamer, M. F. Fox, *Chem. Rev.* **1970**, *70*, 59–93.
[56] Hardsurf program (HS95v09), T. Brinck, **2009**.
[57] K. E. Gutowski, R. D. Rogers, D. A. Dixon, *J. Phys. Chem. B* **2007**, *111*, 4788–4800.
[58] L. Qiu, H. Xiao, X. Gong, X. Ju, W. Zhu. , *J. Hazard. Mater.* **2007**, *141*, 280–288.
[59] D. A. Dixon, D. Feller, K. O. Christe, W. W. Wilson, A. Vij, V. Vij, H. D. Jenkins, R. M. Olson, M. S. Gordon, *J. Am. Chem. Soc.* **2004**, *126*, 834–843.
[60] M. J. Pellerite, R. L. Jackson, J. I. Brauman, *J. Phys. Chem.* **1981**, *85*, 1624–1626.
[61] T. E. Mallouk, G. L. Rosenthal, G. Mueller, R. Brusasco, N. Bartlett, *Inorg. Chem.* **1984**, *23*, 3167–3173.
[62] H. D. Jenkins, H. K. Roobottom, J. Passmore, L. Glasser, *Inorg. Chem.* **1999**, *38*, 3609–3620.
[63] E. F. Byrd, B. M. Rice, *J. Phys. Chem. A* **2009**, *113*, 345–352.
[64] B. J. McBride, S. Gordon, Computer program for calculation of complex chemical equilibrium compositions and applications II, Users manual and program description, NASA, **1996**.
[65] S. Gordon, B. J. McBride, Computer program for calculation of complex chemical equilibrium compositions and applications I, Analysis, NASA, **1994**.

Received: February 16, 2010
Published online: April 29, 2010

